Heliospheric modulation of cosmic rays

Renata Modzelewska[1]

A.Gil[1], A. Wawrzynczak[1], M. Siłuszyk[1], K. Iskra[2], M. Alania[1]

1. **Siedlce University, Siedlce, POLAND**
2. **Polish Air Force University, Deblin, POLAND**

renatam@uph.edu.pl

Warszawa, Astrofizyka Cząstek w Polsce, 20-21 maja 2019

Outline

Galactic cosmic ray (GCR) variations by NM. Solar magnetic (Hale) cycle consisting of two successive 11-year of solar cycle.

27-day anisotropy of GCR.

Recurrent GCR intensity variation. Neutron monitors and PAMELA data. 3-4CRP

Forbush decreases

11-year variation of GCR

Near–Earth air temperatures vs solar activity

Parker transport equation-modeling

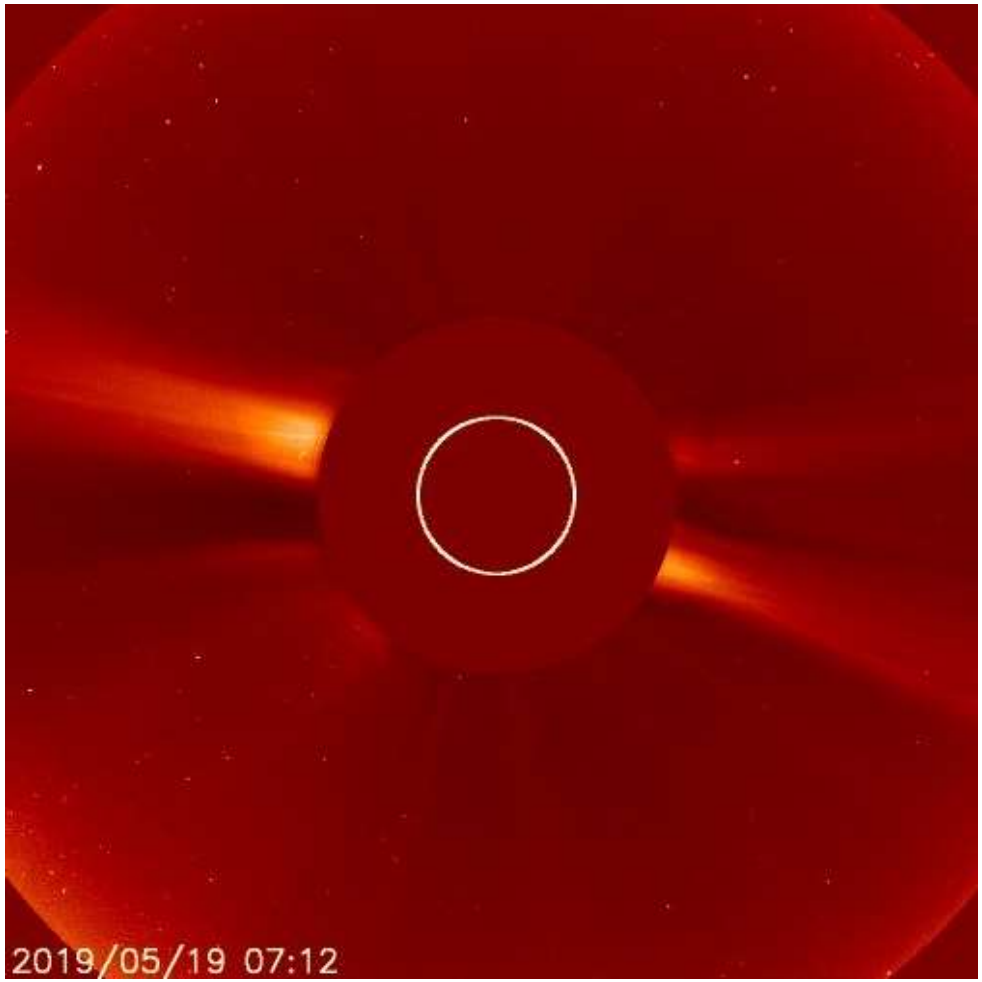

https://www.swpc.noaa.gov/products/lasco-coronagraph

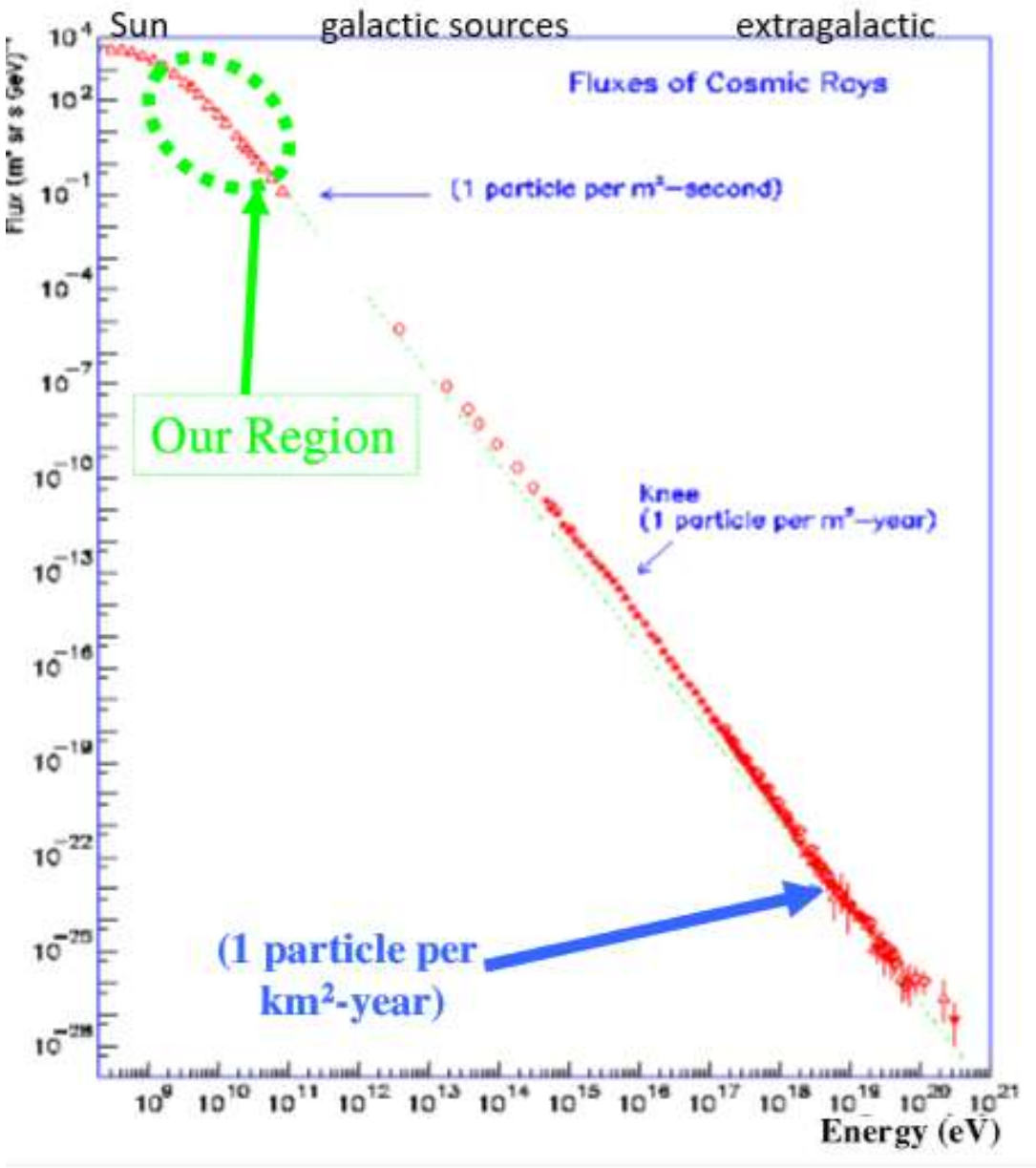

CERN courier, 1999

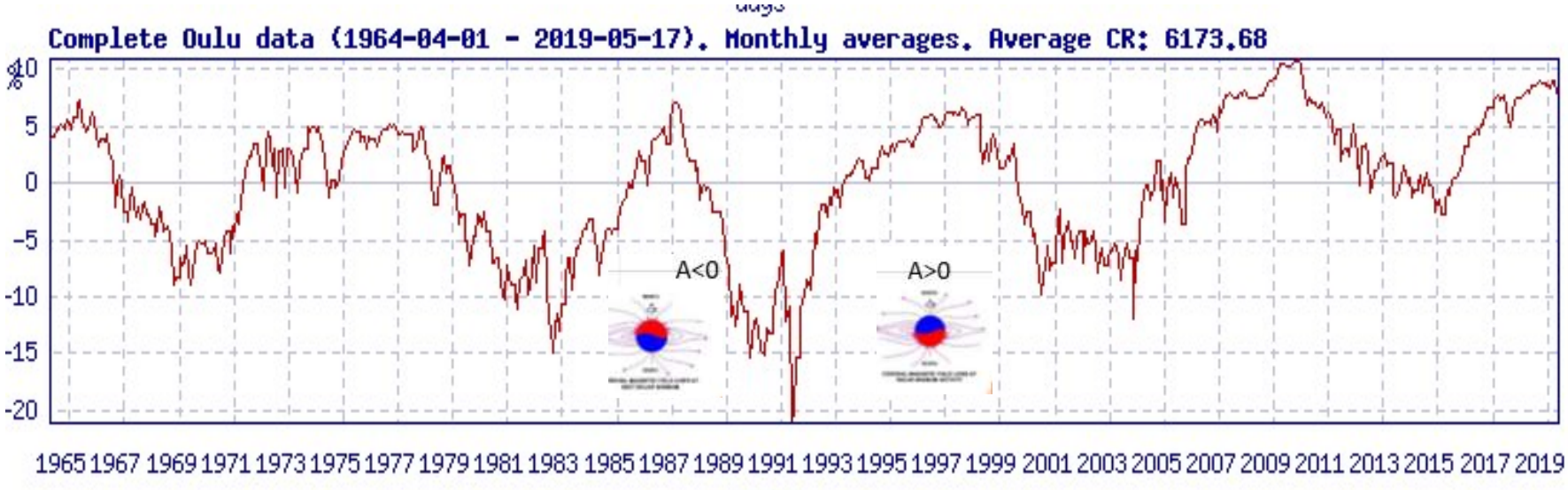
Complete Oulu data (1964-04-01 - 2019-05-17), Monthly averages, Average CR: 6173.68
%
10
5
0
-5
-10
-15
-20
A<0
A>0
1965 1967 1969 1971 1973 1975 1977 1979 1981 1983 1985 1987 1989 1991 1993 1995 1997 1999 2001 2003 2005 2007 2009 2011 2013 2015 2017 2019
years

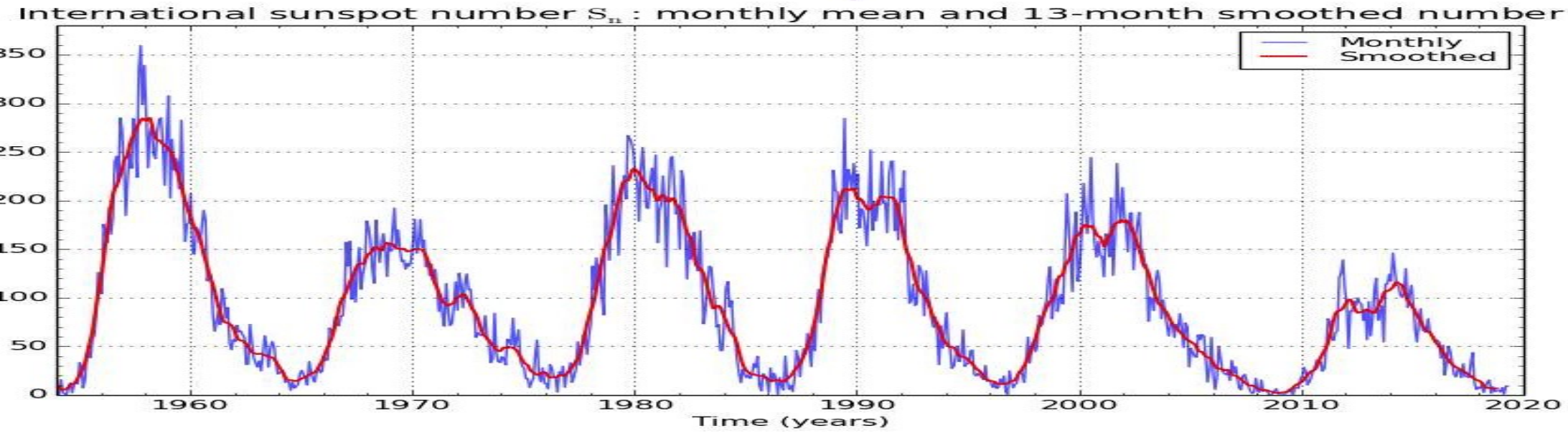
International sunspot number S_n : monthly mean and 13-month smoothed number
Monthly
Smoothed
350
300
250
200
150
100
50
0
1960
1970
1980
1990
2000
2010
2020
Time (years)
SILSO graphics (http://sidc.be/silso) Royal Observatory of Belgium 2019 May 7

Modzelewska and Alania, A&A, 2018:

Temporal changes of the average 2D A27A smoothed over 13 solar rotations for 6 NMs (Moscow, Kiel, Oulu, Deep River, Climax) in 1965-2014 during A>0 and A<0

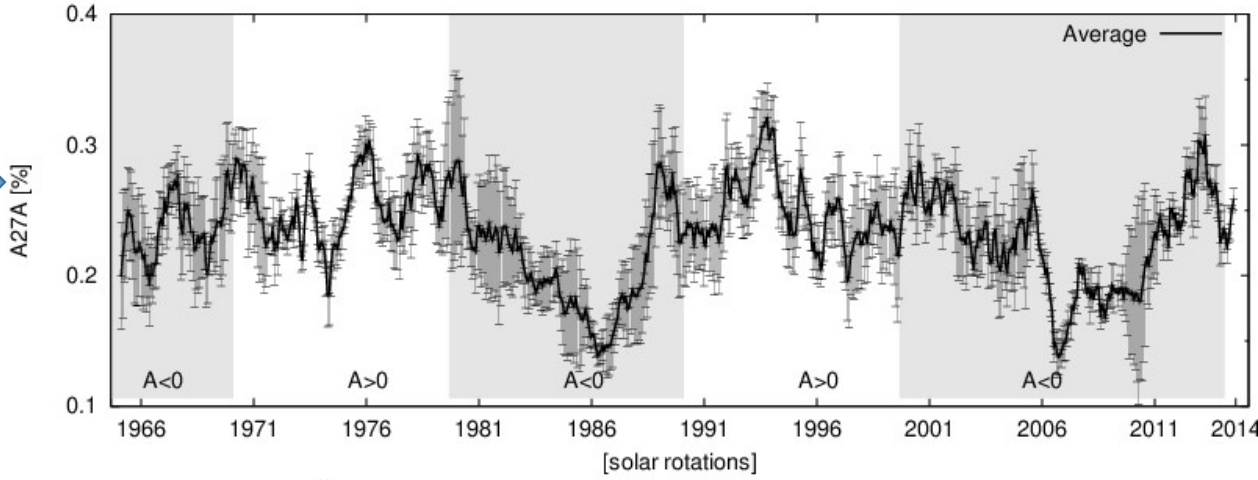

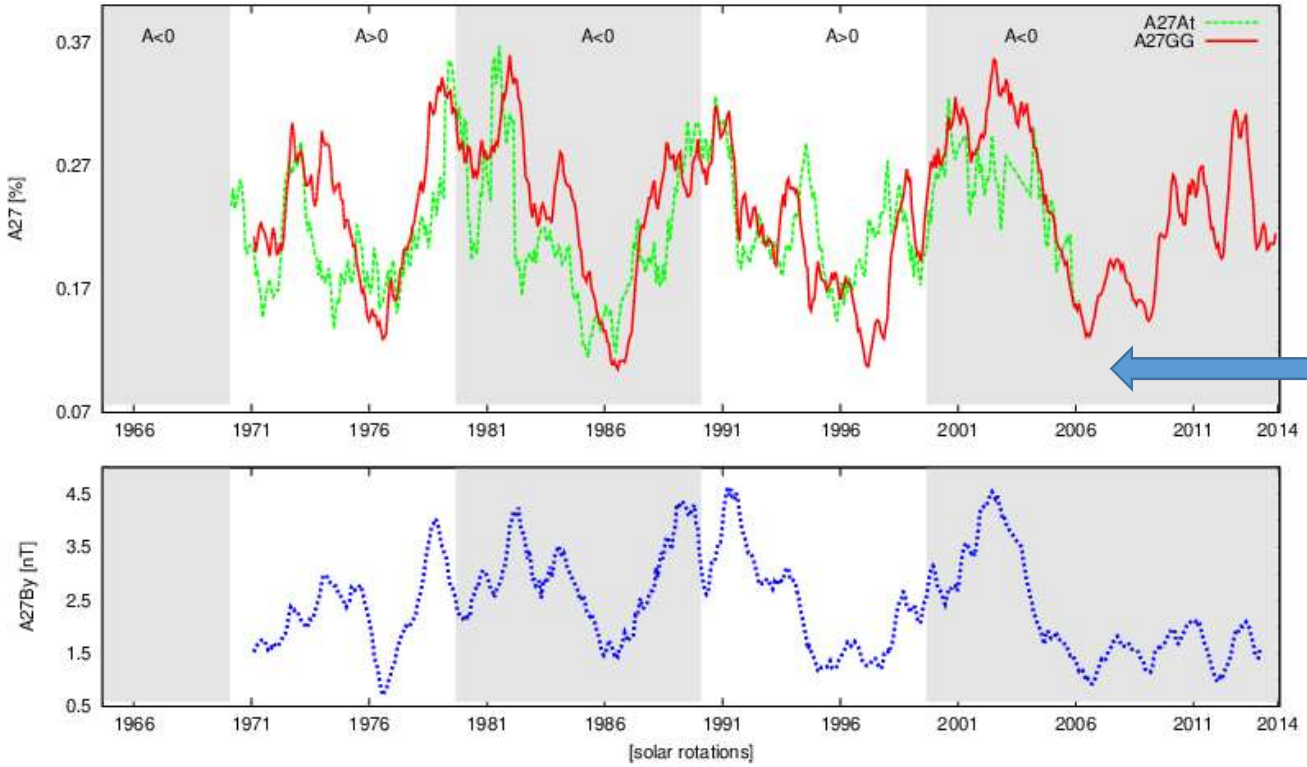

Temporal changes of the amplitudes of the 27-day variation of the GG index and north-south At component of the 3D anisotropy (top) and By component of the HMF (bottom) smoothed over 13 Sun's rotations during A>0 and A<0 polarity epochs.

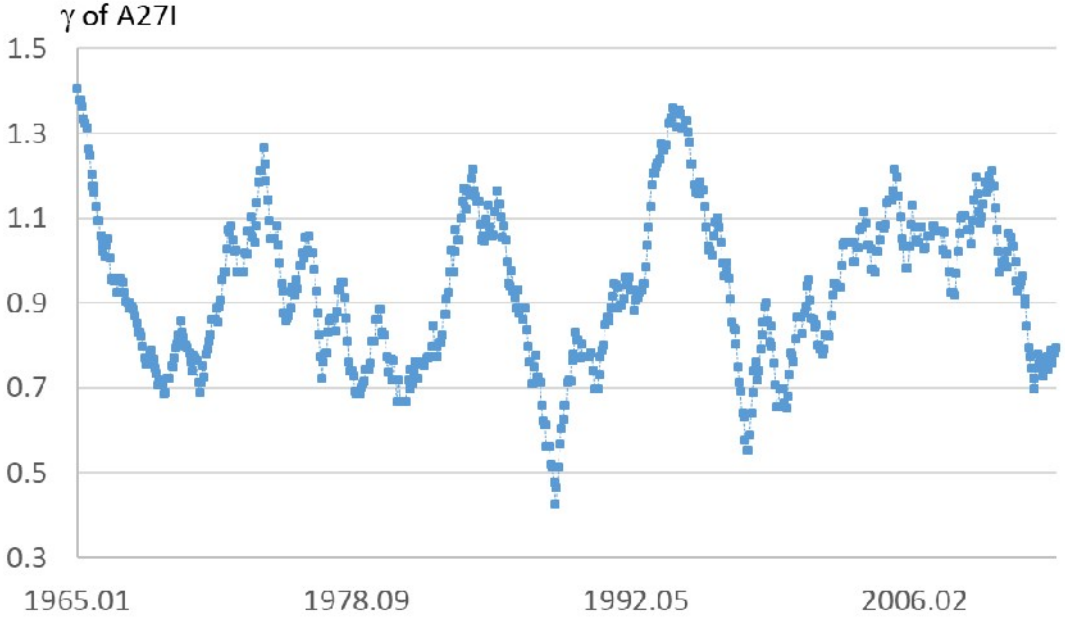

$$\frac{\delta D(R)}{D(R)} = \begin{cases} A R^{-\gamma} \; for \quad R \le R_{\max} \\ 0 \quad for \quad R > R_{\max} \end{cases}$$

Dorman, 1963; Ahluwalia, Ericksen, 1971; Yasue i in., 1982

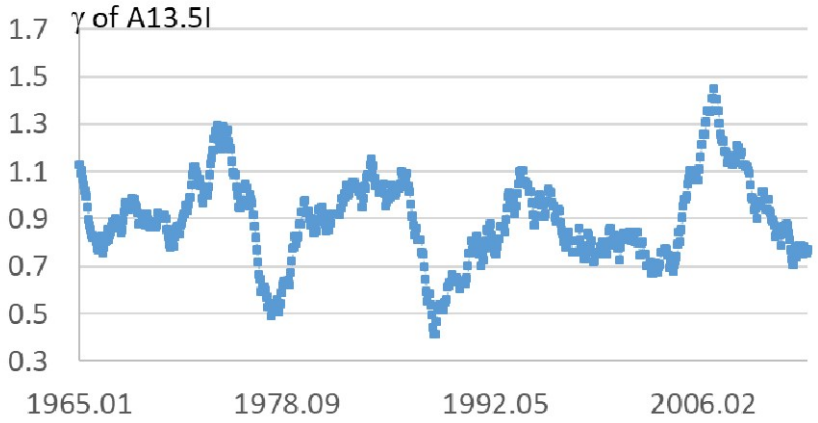

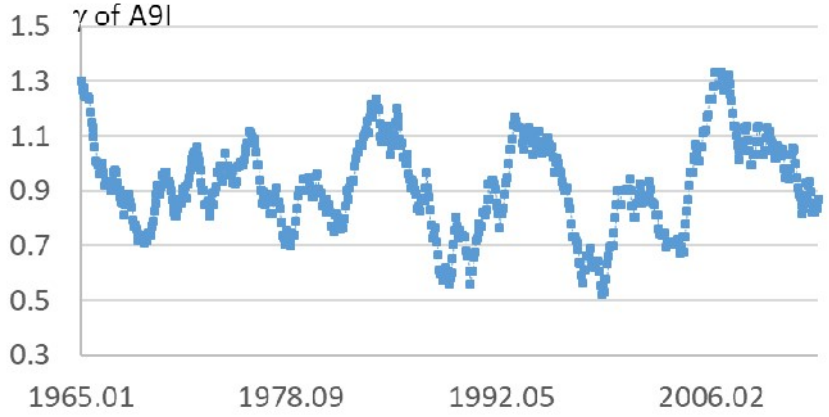

The energy spectrum of the first three harmonics of the 27-day variation of the galactic intensity of cosmic radiation is less steep (more hard) during maxima of solar activity, while in the minima is steeper (soft) and the physical mechanism underlying this phenomenon is proposed.

Gil, Alania, 2016

3-4 CRP

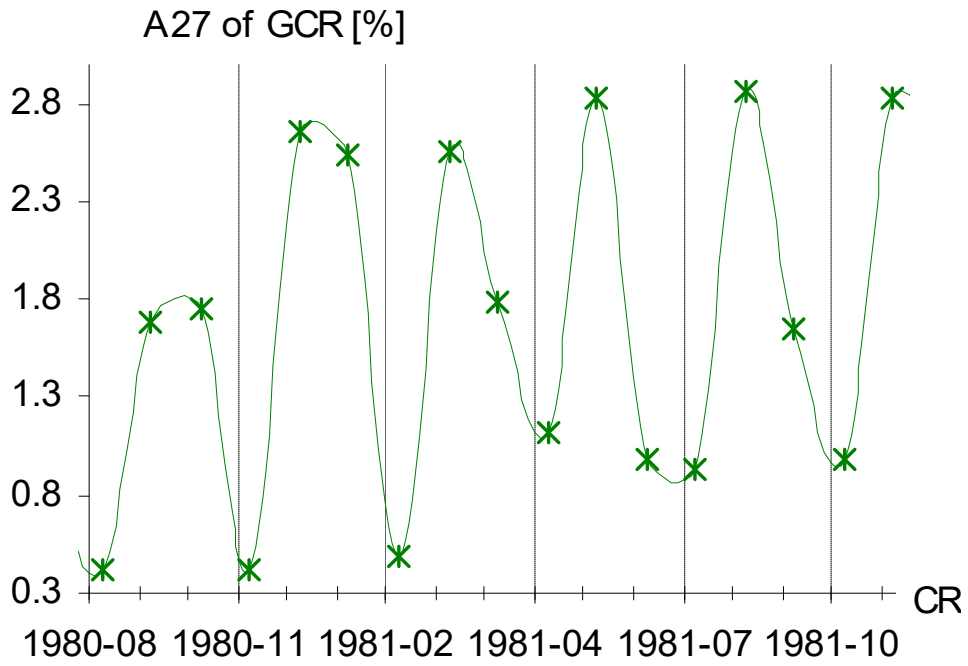

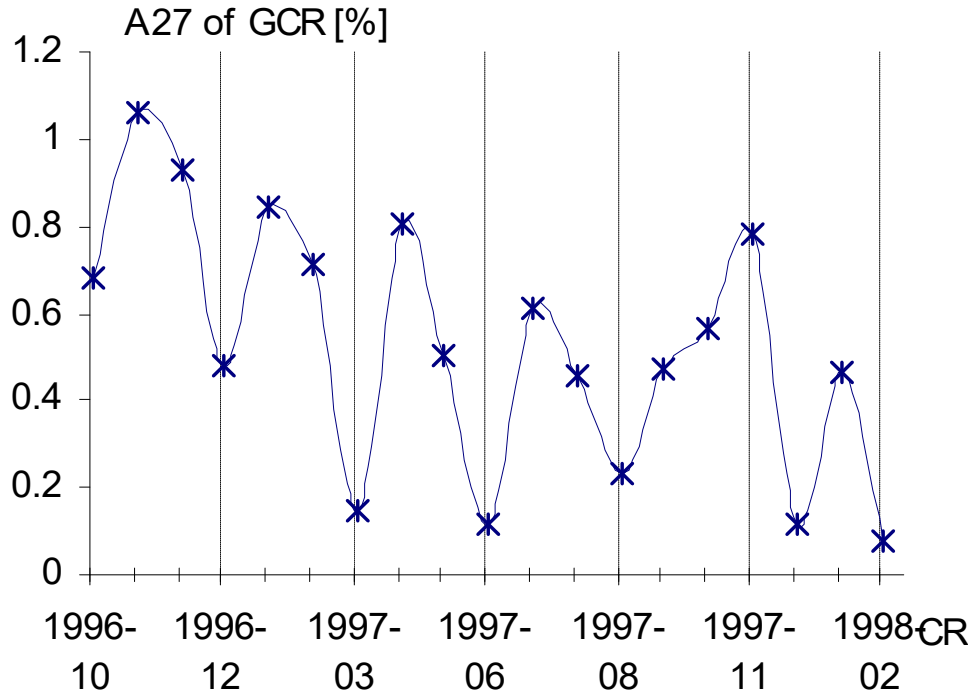

New type of quasi-variability visible both in the GCR and in the parameters of solar activity and solar wind with duration from 3 to 4 Carrington rotations

Gil, Alania, 2013

Modzelewska, Mayorov, Munini, IoP, JPCS, 2019:

Daily PAMELA proton (R=1.8 GV), helium (R=1.7 GV) fluxes, Oulu NM (Rc=0.8 GV) GCR intensity count rates, solar wind velocity V and Bx component of the HMF for 2006-2015

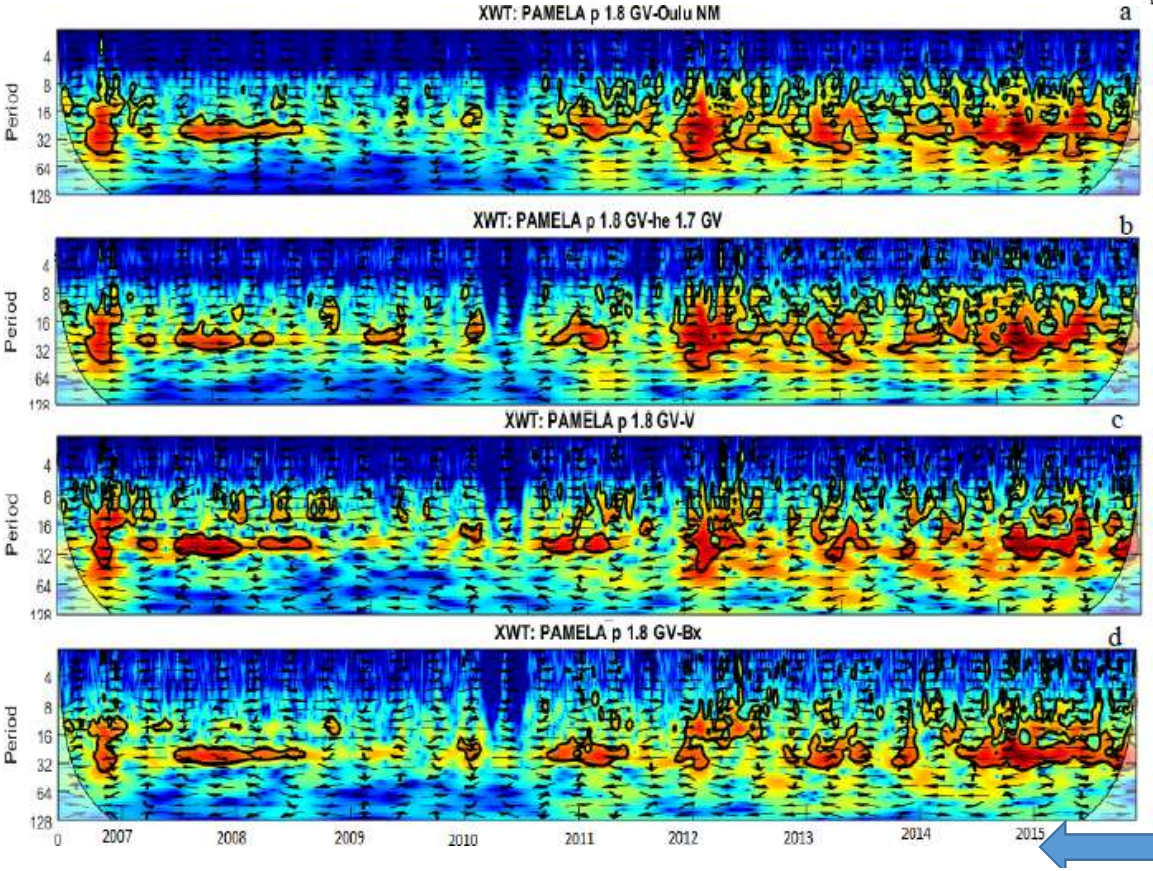

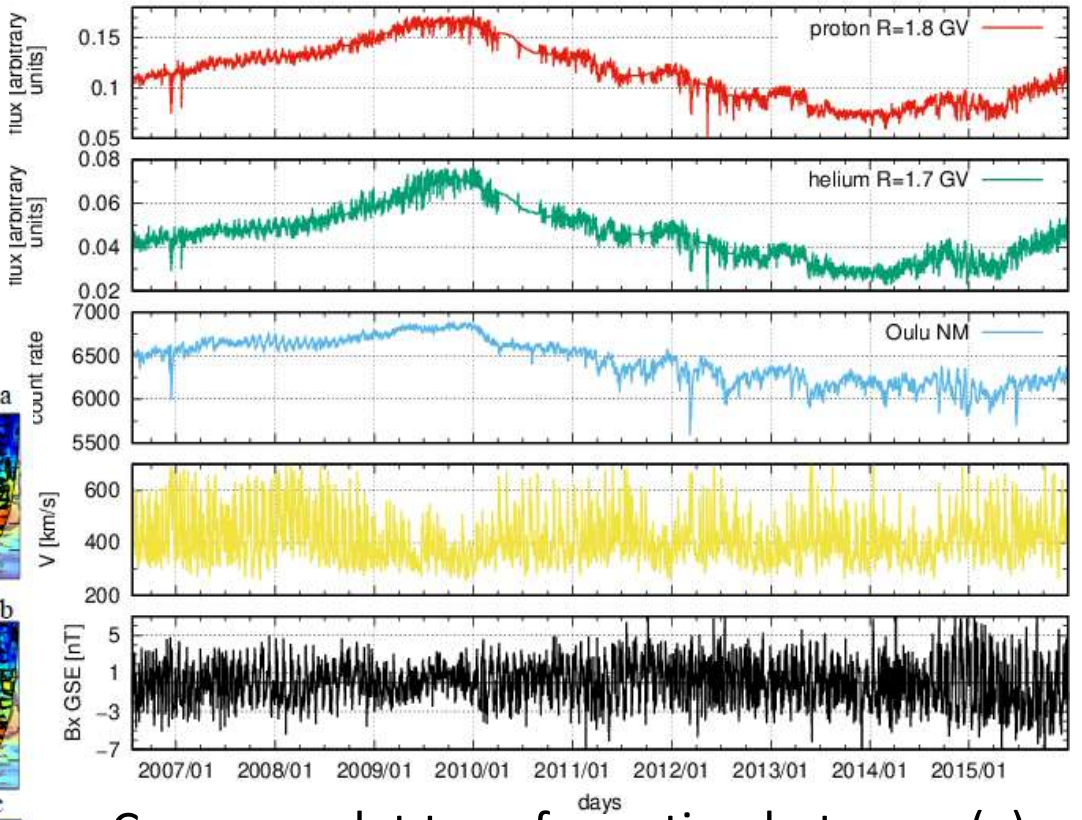

Cross wavelet transformation between (a) PAMELA proton spectra (R=1.8 GV) and Oulu NM data, (b) PAMELA proton spectra (R=1.8 GV) and helium spectra (R=1.7 GV), (c) PAMELA proton spectra (R=1.8 GV) and V and (d) PAMELA proton spectra (R=1.8 GV) and Bx for 2006- 2015.

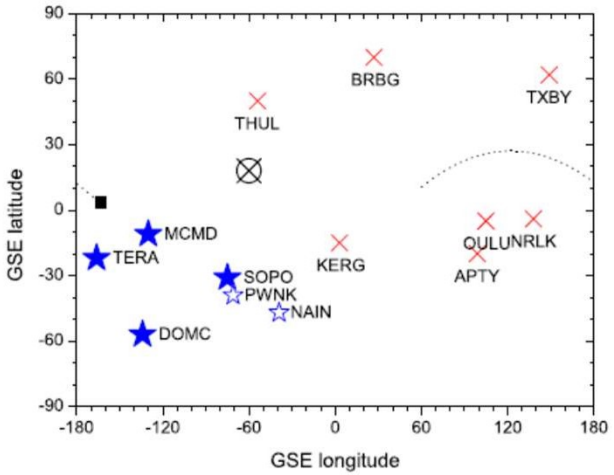

ACRE-anisotropic cosmic-ray enhancement, observed as ~ 5% increase in polar NMs at 12-19 UT 07.06.2015. The amplification was very anisotropic, registered only by neutron monitors with asymptotic directions in the S-W quadrant (blue stars in the left figure).

Gil et al., 2018

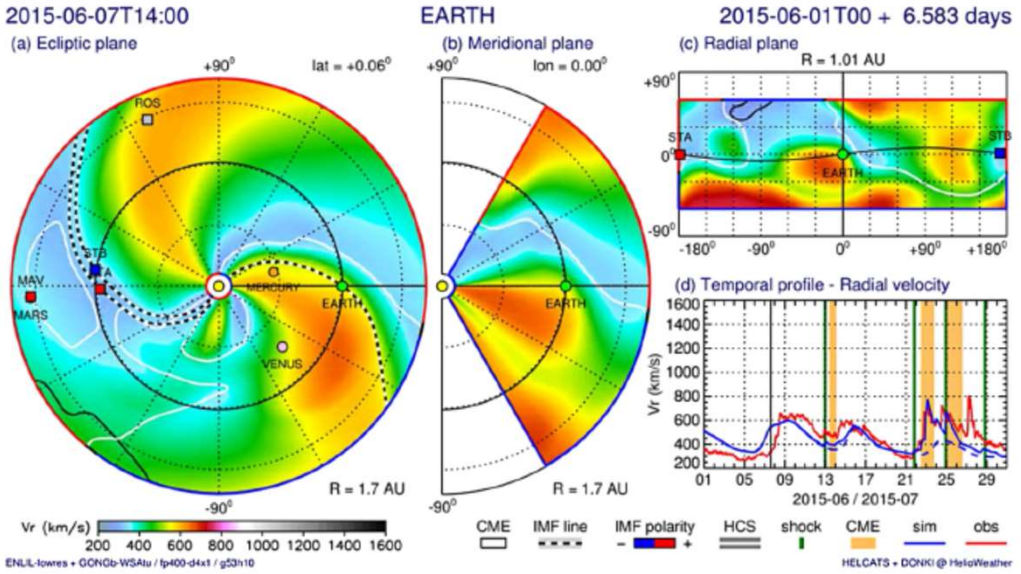

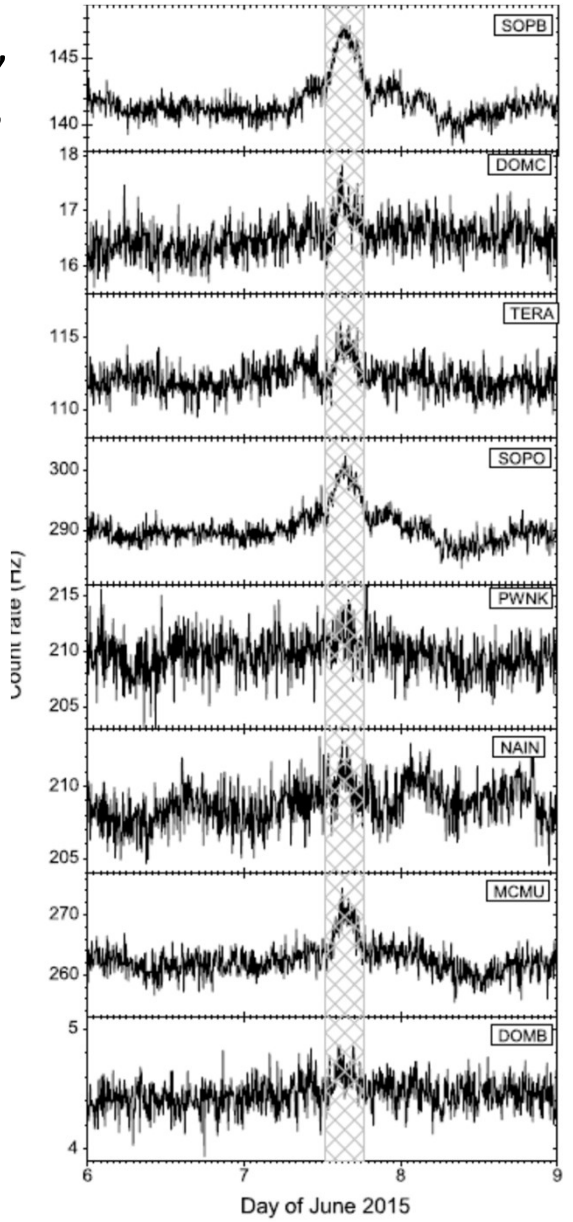

Stochastic model of GCR transport

- In the 3D heliosphere the SDEs equivalent to the forward (lower sign) and backward (upper sign) FPE have a form:

$$
\begin{aligned}
dr &= \left(\frac{2}{r}K^S_{rr} + \frac{\partial K^S_{rr}}{\partial r} + \frac{ctg\theta}{r}K^S_{\theta r} + \frac{1}{r}\frac{\partial K^S_{\theta r}}{\partial \theta} + \frac{1}{rsin\theta}\frac{\partial K^S_{\varphi r}}{\partial \varphi} \pm U \pm v_{d,r}\right)\cdot dt + [B\cdot dW]_r \\
d\theta &= \left(\frac{K^S_{r\theta}}{r^2} + \frac{1}{r}\frac{\partial K^S_{r\theta}}{\partial r} + \frac{1}{r^2}\frac{\partial K^S_{\theta\theta}}{\partial \theta} + \frac{ctg\theta}{r^2}K^S_{\theta\theta} + \frac{1}{r^2 sin\theta}\frac{\partial K^S_{\varphi\theta}}{\partial \varphi} \pm \frac{1}{r}v_{d,\theta}\right)\cdot dt + [B\cdot dW]_\theta \\
d\varphi &= \left(\frac{K^S_{r\varphi}}{r^2 sin\theta} + \frac{1}{rsin\theta}\frac{\partial K^S_{r\varphi}}{\partial r} + \frac{1}{r^2 sin\theta}\frac{\partial K^S_{\theta\varphi}}{\partial \theta} + \frac{1}{r^2 sin^2\theta}\frac{\partial K^S_{\varphi\varphi}}{\partial \varphi} \pm \frac{1}{rsin\theta}v_{d,\varphi}\right)\cdot dt + [B\cdot dW]_\varphi \\
dR &= \mp\frac{R}{3}(\vec{\nabla}\cdot U)\cdot dt
\end{aligned}
$$

Wawrzynczak, Modzelewska & Gil, 2018

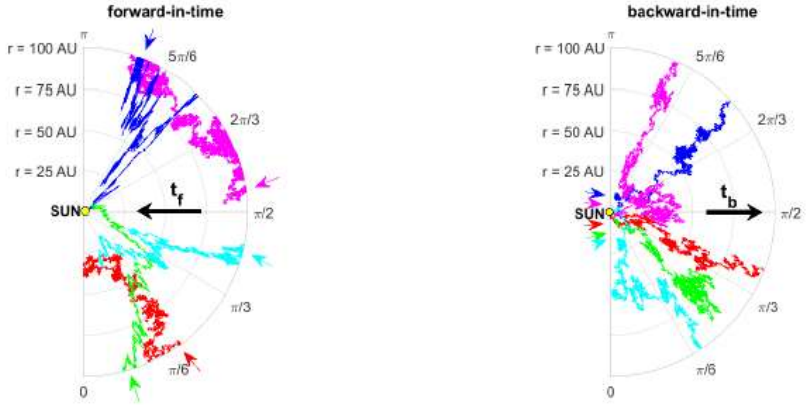

Fig.2. Schematic illustration of the pseudoparticles trajectories projected on a 2D plane in the forward-in-time and backward-in-time approach to the FPE solution. The initial position of pseudoparticles is marked by an arrow in color corresponding to trajectory's color. In the backward-in-time scenario, all pseudoparticles are initialized at the same point. The black arrow signalized how time passes from the pseudoparticles perspective.

Stochastic model of GCR transport , comparison for 1D, 2D and 3D model

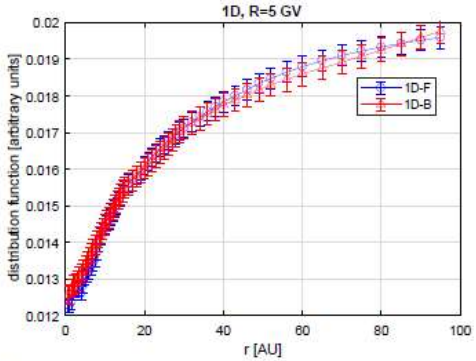

Fig.1. The expected profile of the distribution function $f(\vec{r}, R)$ with respect the radial distance r obtained from the forward- and backward-in-time solutions of the FPE in 1D heliosphere.

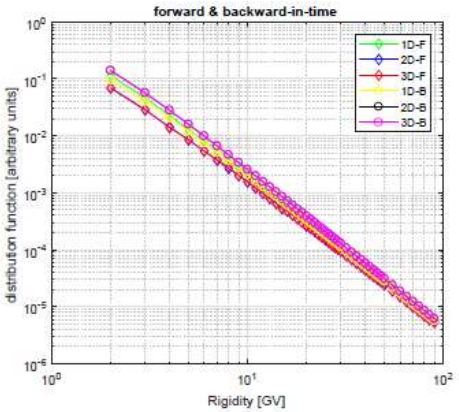

Fig.3. The expected profile of the distribution function $f(\vec{r}, R)$ with respect the particles rigidity R obtained from the forward- and backward-in-time solutions of the FPE in 1D, 2D and 3D heliosphere.

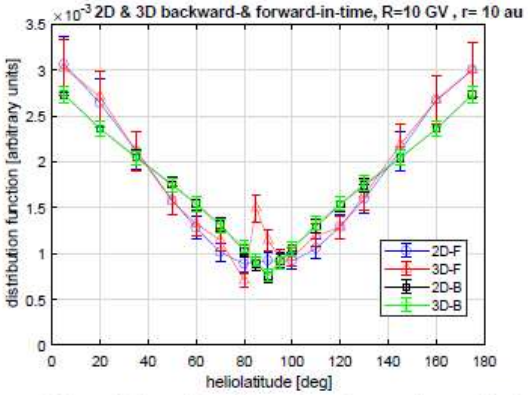

Fig.4. The expected profile of the distribution function $f(\vec{r}, R)$ with respect the heliolatitude θ obtained from the forward- and backward-in-time solutions of the FPE in 2D and 3D heliosphere.

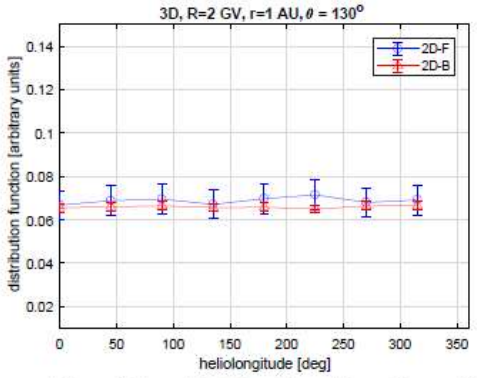

Fig.5. The expected profile of the distribution function $f(\vec{r}, R)$ with respect the heliolongitude φ obtained from the forward- and backward-in-time solutions of the FPE in 3D heliosphere.

Wawrzynczak, Modzelewska & Gil, 2018

Estimation of the $_{KII}$ during Forbush decrease by Approximate Bayesian Computation (ABC)

- The ABC SMC method was used to estimate the most probable set of parameters of the paralel diffusion coefficient K_{II} during the modeled Fd.
- The formula proposed for the diffusion coefficient K_{II} contains the rigidity dependence of the rigidity spectrum exponent during Fd $\gamma = \gamma(R)$.

$$\gamma(R) = \begin{cases} \alpha - \beta \cdot \tau^{\delta} \cdot exp(\eta \cdot \tau) \cdot R^{\zeta}; & within \quad disturbed \quad region, \\ \alpha; & outside \quad disturbed \quad region. \end{cases}$$

- The experimental study have some methodical limitations, which impede to derive the specific formulas thus ABC SMC algorithm was employed to estimate the values of $\gamma = \gamma(R)$ parameters giving the best fit of the Fd model with the experimental data as:

$$\rho(d^{Fd_{data}}, d_{obs}^{Fd_{data}}) = \frac{1}{K}\sum_{k}^{K}\left(\frac{1}{NM}\sum_{R}^{NM_s}\frac{|I_R^k - \hat{I}_R^k|}{I_R^k + \hat{I}_R^k}\right),$$

where K- Fd data samples (days), NM - number of NM data (in model various R), $\hat{I}_R^k$- is the Fd amplitude reported by R-th neutron monitor on k-time (day) and I_R^k - corresponding modelled Fd amplitude.

- In calculations, we have used the GCR daily intensities recorded by the four neutron monitors and Nagoya muon telescope during the Fd event on 5–21 November 2004.

Estimation of the $_{KII}$ during Forbush decrease by Approximate Bayesian Computation (ABC)

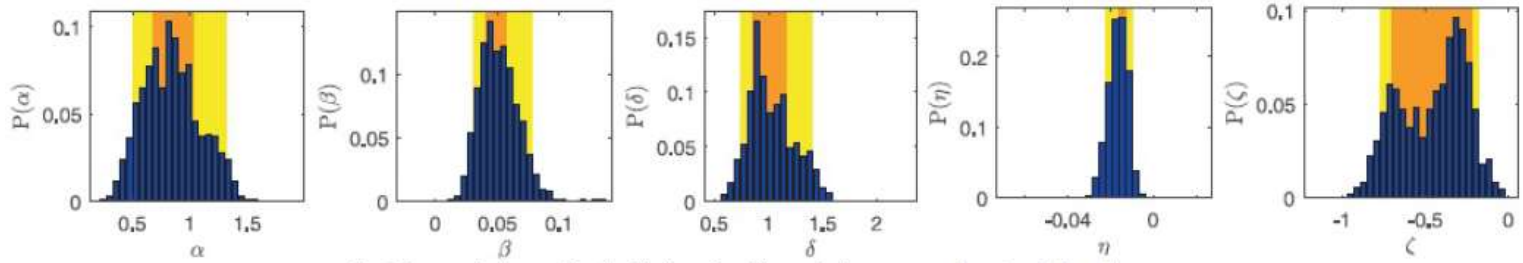

Fig. The marginal posterior distributions for all searched parameters $\lambda \equiv (\alpha, \beta, \delta, \eta, \zeta)$

- The performed computations allowed to estimate with reasonable statistics all five parameters of the diffusion coefficient.
- Moreover, the results confirm that during the Fd in November 2004 there existed the power-law dependence of exponent γ on rigidity in the form $\gamma(R) \propto R^{-0.3}$.

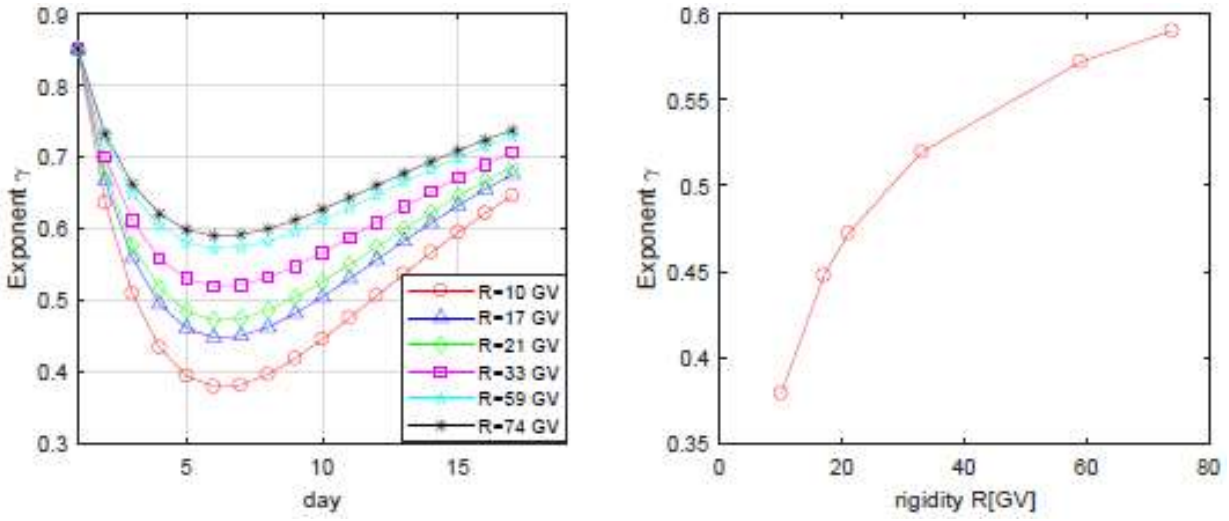

Fig. The profile of the exponent γ calculated with use of the estimated by the ABC SMC algorithm values of most probable parameters .

Wawrzynczak & Kopka, 2018

Long period 11-years GCR variations

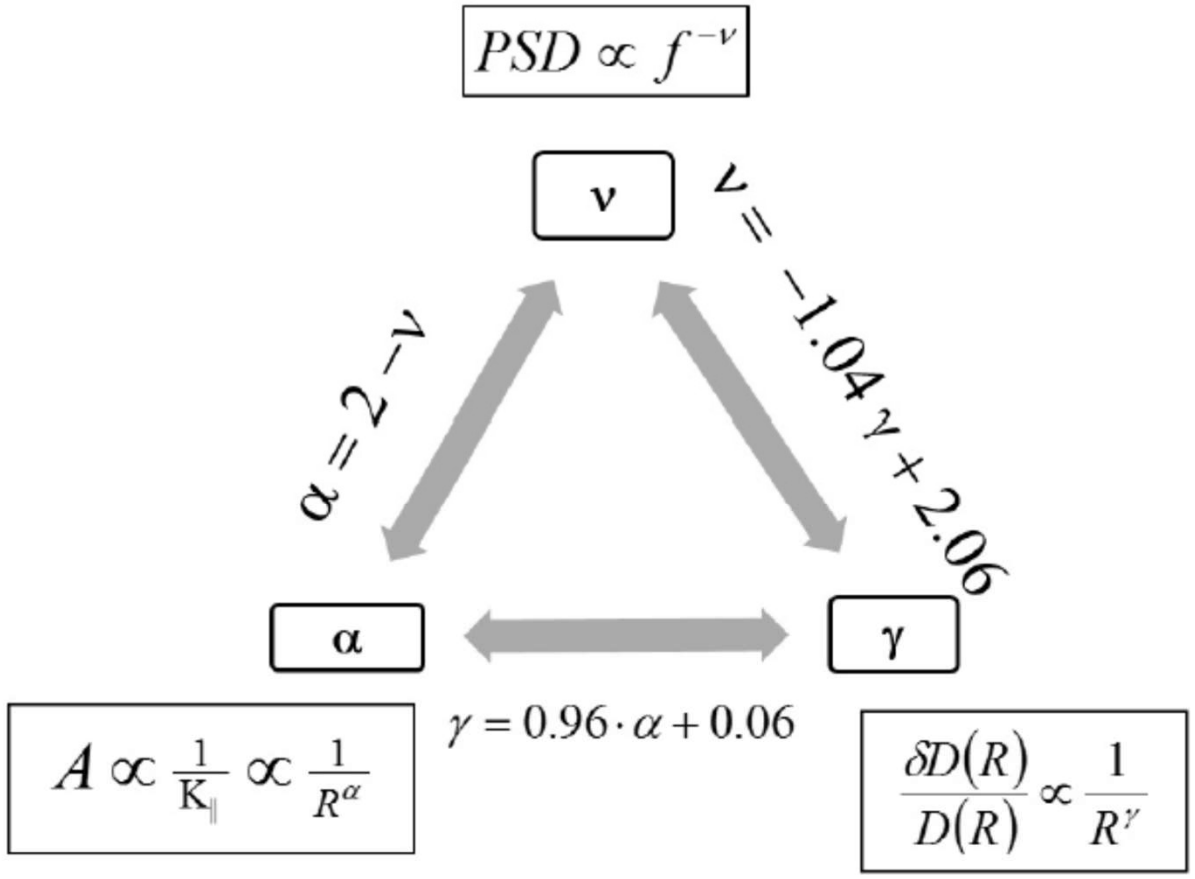

The diagram demonstrate relations between parameters: γ, ν and α.

Long period 11-years GCR variations

The resonant frequency calculated for the GCR particles of rigidity 10 GV regularly decreases during minima and increases during maxima epochs of SA for the total of the considered period between 1969 and 2011. The paper proves that the long-term variations in the HMF intensity and fluctuation levels play a decisive role, while the contribution of the SW speed is not important.

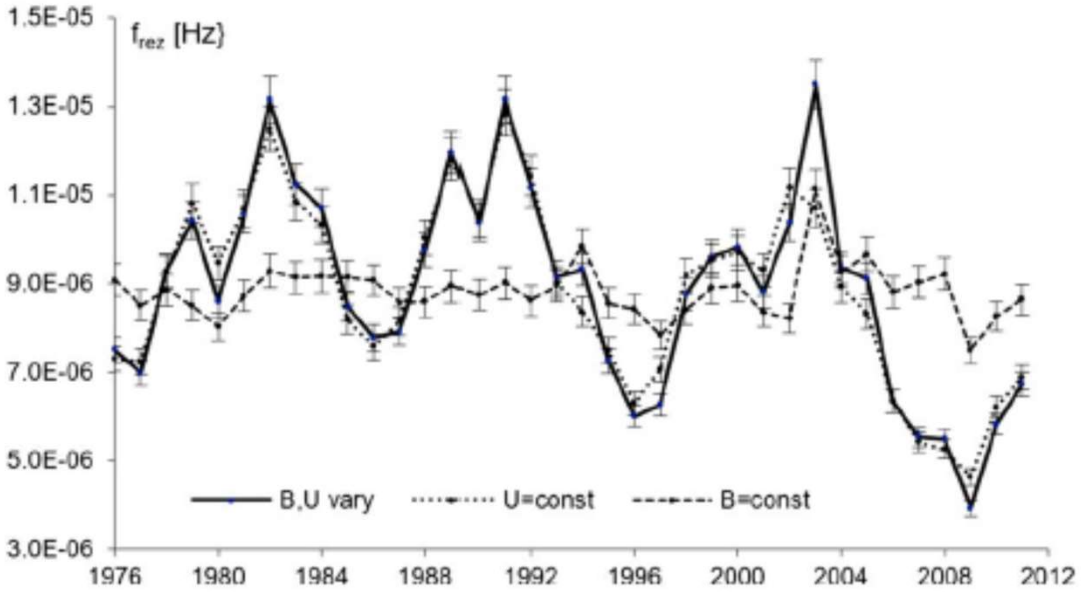

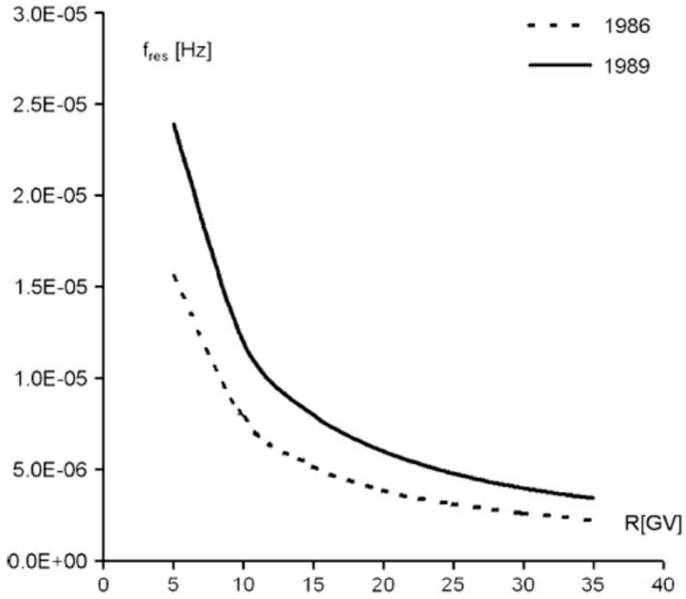

Figure 2. Yearly alternations of the resonant frequency f_{res} for rigidities 10 GV of GCR protons in different cycles of SA between 1976 and 2011; (a) the solid line—B and U_{SW} vary, (b) the dotted line—B varies and U_{SW} is constant, and (c) the dash line—U_{SW} varies and B is constant with the cycle of SA.

$$f_{res} = \frac{300}{2\pi} \frac{U_{SW} \cdot B}{R},$$

Siluszyk, Alania, Iskra, JGR, 2018

The new 2-D time dependent models of the 11–year variation was developed. This model implements the physical parameters characterizing the temporal changes of the magnitude *B* of the IMF, tilt angle d of the HNS and parameters: γ and ν for the last 4 solar cycles: from #20 to #23.

In the models temporal changes of the rigidity spectrum exponent γ, characterizing a rigidity dependence of amplitudes of the 11–year variations of the GCR intensity, and the exponent ν of the PSD of the HMF turbulence were implemented as proxies.

The temporal changes of the physical parameters implemented in the 2-D model have different delay times with respect to the temporal changes of the smoothed experimental data of the GCR intensity observed by NM Oulu.

We obtained different delay time for the solar cycles: from #20 to #23 - an acceptable compatibility is kept when the minimum of the expected temporal changes of the GCR particles density is shifted with respect to the minimum of the temporal changes of the smoothed experimental data of the GCR intensity.

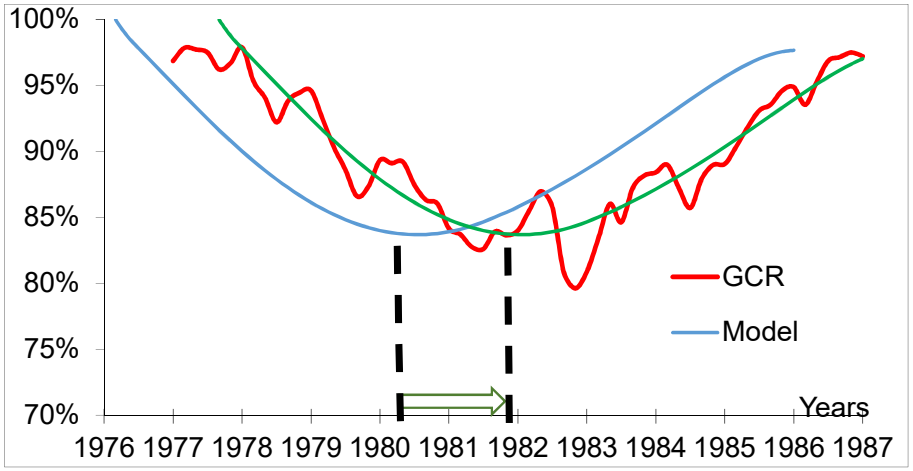

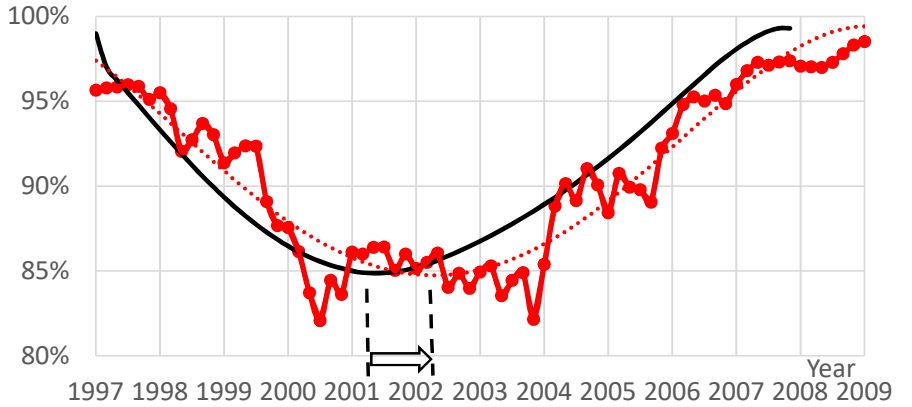

Solar cycle	from	to	Duration	Delay time
20	1964	1976	11.4	4
21	1976	1986	10.5	18
22	1986	1996	9.9	2
23	1996	2008	12.3	12

In figure are presented time profiles of the intensity of GCR for Kiel neutron monitor and sunspot number from 1959 to 2014. This period is divided into five periods

No	Period	Cycles	r(SSN ; I_{GCR})	dr	d(SSN; I_{GCR}) [months]
I	1959.00-1969.42	A<0	-0,89	0.03	15-17
II	1971.58-1979.83	A>0	-0,84	0.04	2
III	1980.33-1990.00	A<0	-0,90	0.03	6
IV	1991.33-1999.67	A>0	-0,94	0.02	4
V	2000.42-2012.33	A<0	-0,94	0.02	13-14

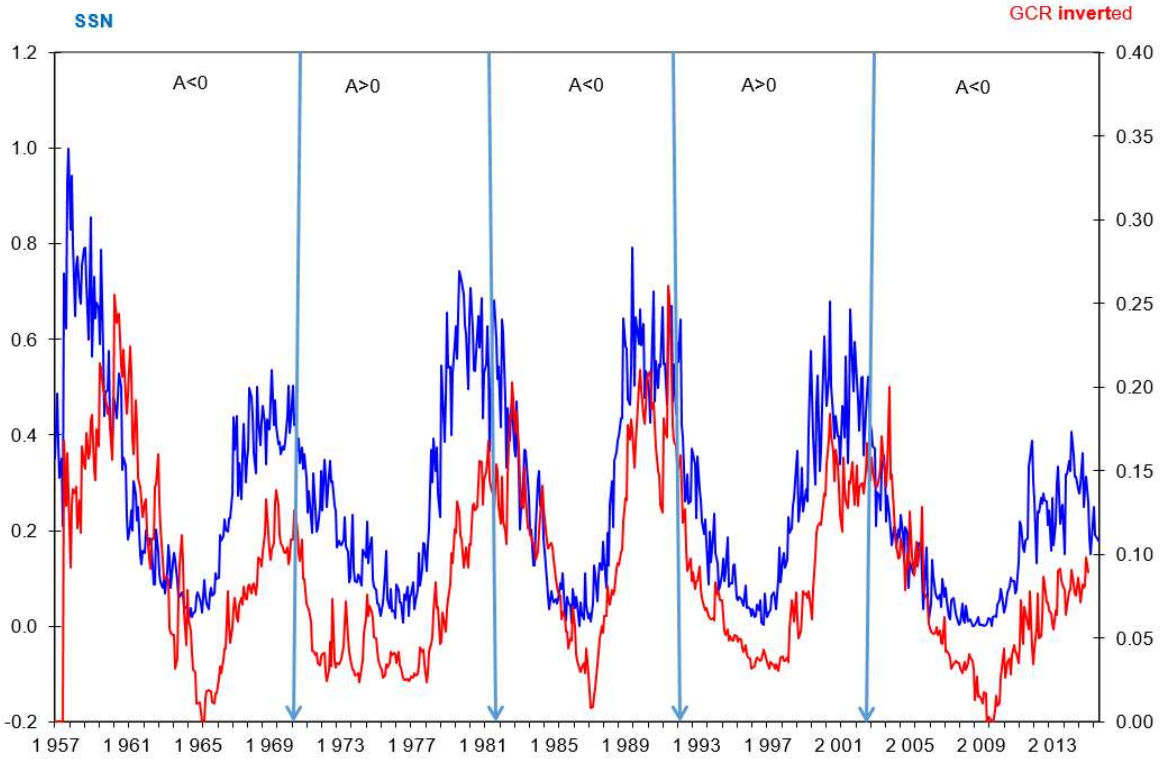

No	Period	Cycles	r(SSN ; I_{GCR})	dR	d(SSN; I_{GCR}) [months]
I	1959-1965	A<0 ↗	0.91	0.03	15--16
II	1965-1968	A<0 ↘	0.88	0.05	5
III	1971-1976	↗ A>0	0.40	0.08	0
IV	1976-1978	↘ A>0	0.84	0.06	1
V	1981-1987	A<0↗	0.87	0.04	10--11
VI	1987-1988	A<0 ↘	0.96	0.04	4--5
VII	1991-1997	↗ A>0	0.92	0.03	0
VIII	1997-1999	↘ A>0	0.86	0.06	4--5
IX	2002-2009	A<0↗	0.93	0.03	13--14
X	2009-2013	A<0 ↘	0.80	0.06	1

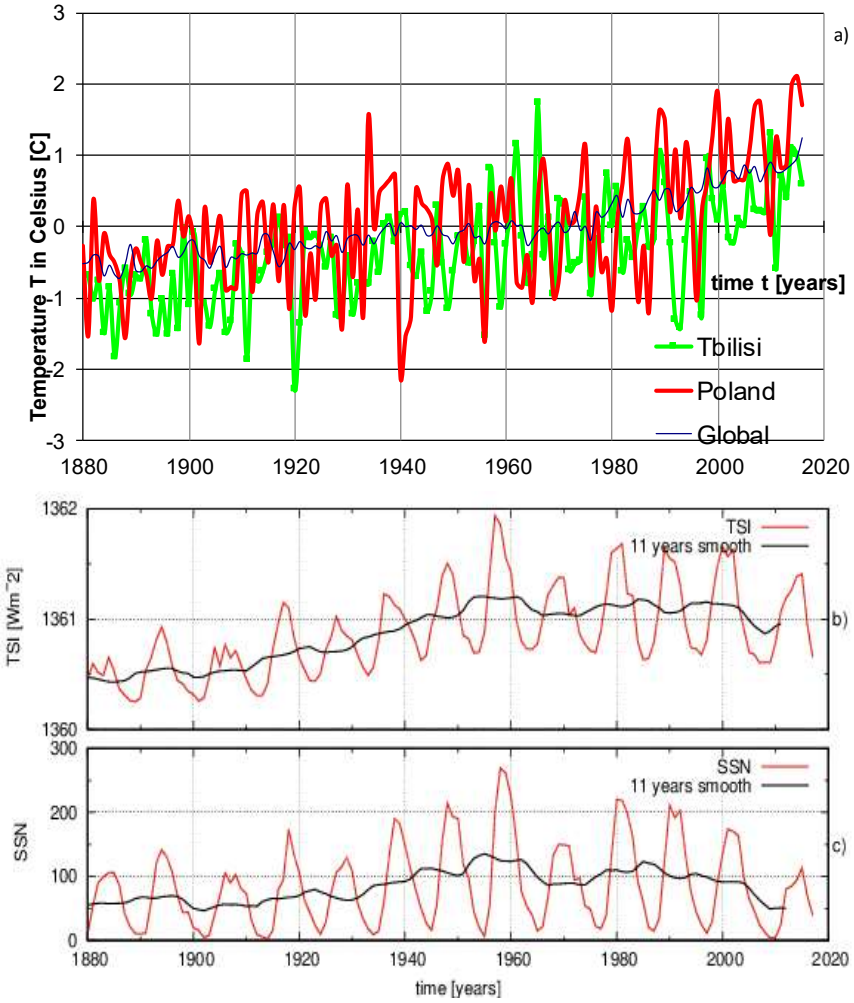

Temporal changes of the (a) annual near-surface air temperature T in Poland (red), Tbilisi (green) and global air temperature (black); (b) annual total solar irradiance TSI and (c) SSN in 1881-2016

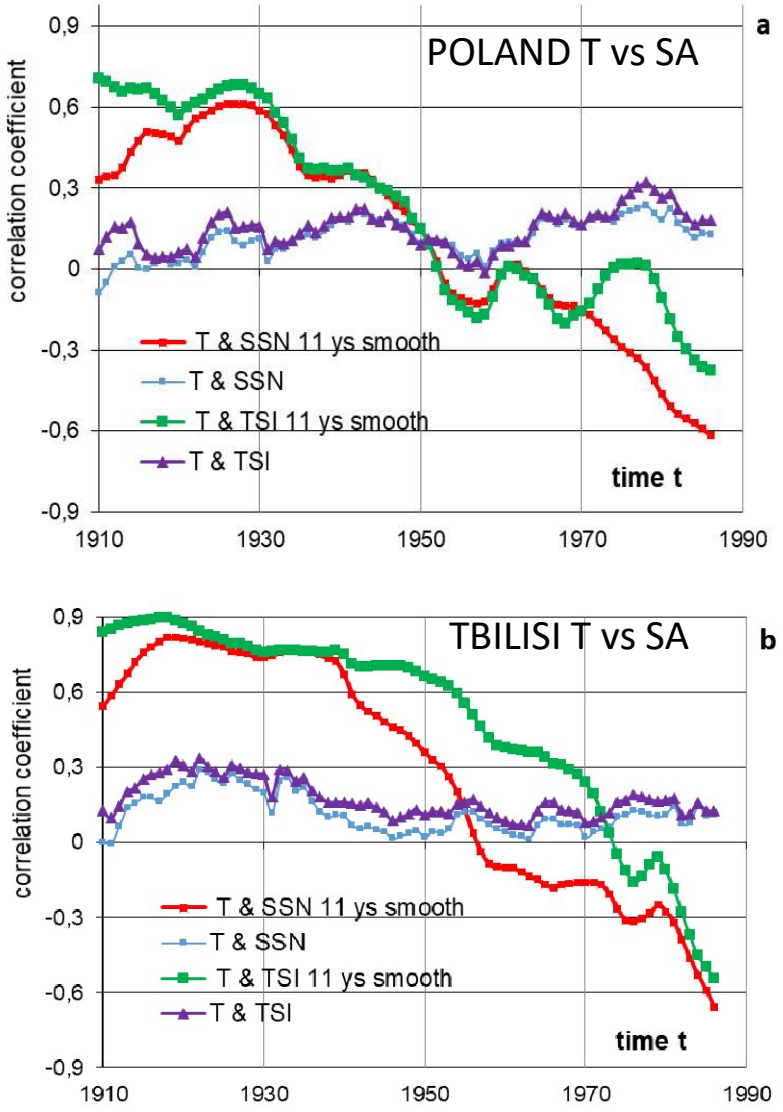

Temporal changes of the correlation coefficients between: annual near-surface air tempeature T and SSN (T&SSN, blue), T&SSN for 11-years smoothed data (red), annual near-surface air tempeature T and TSI (T&TSI, violet), T&TSI for 11-years smoothed data (green) for Poland (a) and Tbilisi (b) for 1911-1986.

Conclusions:

1. Amplitude of the 2D ecliptic 27-day GCR anisotropy is polarity dependent, larger values for positive polarity, while north-south component of the 27-day GCR anisotropy does not depend on solar magnetic polarity.
2. The energy spectrum of the first three harmonics of the 27-day variation of GCR intensity is hard in maximum epochs of solar activity and soft during solar minima.
3. New type of the GCR quasi-variability with duration from 3 to 4 Carrington rotations is caused by the turbulent solar dynamo.
4. We have scanned the diffusion coefficient parameters space by ABC algorithm to estimate the value of parameters giving the best fit of the Fd model with the experimental data. This methodology allowed to confirm that during the Fd in November 2004 exists the postulated rigidity dependence of the rigidity spectrum exponent in the form $\gamma(R) \propto R^{-0.3}$
5. The time interval ~70 years (1890-1960) decisively contributes in creation of global warming effect, when a correlation coefficient between changes of solar activity and T is very high.

Future work plan:

- **GCR variations in the whole solar cycle 24 and solar minimum 24/25**
- **Rigidity dependence of the 27-day GCR amplitude using PAMELA and ARINA data (2006-2016), comparison with NMs**
- **The explanation of a mechanism which causes QBO of GCR.**
- **Studies of other ACRE events.**
- **Checking whether the estimated rigidity dependence of exponent γ is visible in other registered Fds and/or there are required some conditions to be fulfilled like e.g., the relevant amplitude of Fd, the size of modulation region.**
- **Delay time problem between solar activity and long term GCR variations: theory and observations**
- **GCR Anisotropy problem-e.g. drift effect in cosmic ray transport etc.**

Thank you!

Acknowledgements:
Investigators of neutron monitor stations, http://www01.nmdb.eu/
PAMELA mission, http://hep.fi.infn.it/PAMELA/
SSN, solar wind and solar data are from http://omniweb.gsfc.nasa.gov

This work was supported by the Polish National Science Centre:

DEC-2012/07/D/ST6/02488 - SONATA
DEC-2016/22/E/HS5/00406 - SONATA BIS
2017/01/X/ST9/01023 - MINIATURA